Super-Resolution UWB Radar Imaging Algorithm Based on Frequency Domain Interferometer

Shouhei Kidera and Tetsuo Kirimoto

Graduate School of Informatics and Engineering, University of Electro-Communications, Tokyo, Japan.
Email: kidera@ee.uec.ac.jp

***Abstract*—Near field radar employing UWB (Ultra Wideband) signals with its high range resolution has great promise for various sensing applications. It enables non-contact measurement of precision devices with specular surfaces like an aircraft fuselage and wing, or a robotic sensor that can identify a human body in invisible situations. As one of the most promising radar algorithms, the RPM (Range Points Migration) was proposed. This achieves fast and accurate surface extraction, even for complex-shaped objects, by eliminating the difficulty of connecting range points. However, in the case of a more complex shape whose variation scale is less than a pulsewidth, it still suffers from image distortion caused by multiple interference signals with different waveforms. As a substantial solution, this paper proposes a novel range extraction algorithm by extending the Capon method, known as FDI (Frequency Domain Interferometry). This algorithm combines reference signal optimization with the original Capon method to enhance the accuracy and resolution for an observed range into which a deformed waveform model is introduced. The results obtained from numerical simulations and an experiment with bi-static extension of the RPM prove that super-resolution UWB radar imaging is accomplished by the combination between the RPM and the extended Capon methods, even for an extremely complex-surface target including edges.**

***Index Terms*—UWB radars, Frequency domain interferometry, Capon method, Reference signal optimization, Super-resolution imaging, Range Points Migration**

I. Introduction

UWB pulse radar with high range resolution has promise for near field sensing techniques. It is applicable to non-contact measurement for reflector antennas or aircraft bodies and wings that have high-precision and specular surfaces, or to robotic sensors that can identify a human body or materials, even in a dark smog in disaster areas. While various kinds of high-resolution radar algorithms have been developed [1], [2], [3], they are not suitable for the above applications because of the large amount of calculation burden or inadequate image resolution. To overcome these problems, we have already proposed some of imaging algorithms, which accomplish a real-time and high resolution surface extraction beyond wavelength [4], [5], [6]. As a high-speed and accurate 3-D imaging method applicable to various target shapes, the RPM algorithm has been proposed [7]. This algorithm directly estimates an accurate direction of arrival (DOA) with a global characteristic of observed range points, instead of connecting them. Then, it offers an accurate target surface, even if the extremely complicated range map is given.

However, this method suffers from a serious image distortion in the case of a more complicated target which has a surface variation less than wavelength, or has many convex and concave edges. This distortion is caused by the richly interfered signals scattered from the multiple scattering centers on the target surface. These components are received within a range scale less than wavelength, and are hardly separated by the former range extraction method, the Wiener filter.

To overcome this problem, this paper proposes a novel range extraction algorithm by extending the Capon method. While the Capon is useful for enhancing the range resolution based on the frequency domain interferometry (FDI) [8], the resolution and accuracy of this method significantly depend on the reference waveform such as a transmitted one. In general, the scattered waveform from the target with wavelength scale differs from the transmitted one [9], and the range resolution given by the original Capon method distorts due to this deformation. To outperform the original Capon, this paper extends the original Capon, which optimizes the reference signal based on the simplified waveform model. The results from numerical simulations and an experiment using the UWB module prove that super-resolution imaging is accomplished by the combination between the RPM and the proposed method.

II. System Model

Fig. 1 shows the system model. It assumes the mono-static radar, and an omni-directional antenna is scanned on the plane, $z = 0$. It is assumed that the target has an arbitrary shape with a clear boundary. The propagation speed of the radio wave c is assumed to be known constant. A mono-cycle pulse is used as the transmitting current. The real space in which the target and antenna are located, is expressed by the parameter (x, y, z). It assumes a linear polarization in the direction of the x-axis. We assume $z \geq 0$ for simplicity. $s'(X, Y, Z')$ is defined as the received electric field at the antenna location $(x, y, z) = (X, Y, 0)$, where $Z' = \mathrm{c}t/(2\lambda)$ is a function of time t.

III. RPM Algorithm

As one of the most promising algorithms applicable to various 3-D target shapes, the RPM algorithm which makes use of a characteristic of global distribution of observed range maps, has been proposed [7]. This assumes that a target boundary point (x, y, z) exists on a sphere with center $(X, Y, 0)$ and

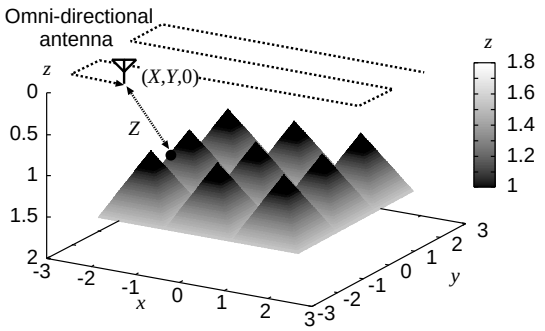

Fig. 1. System model.

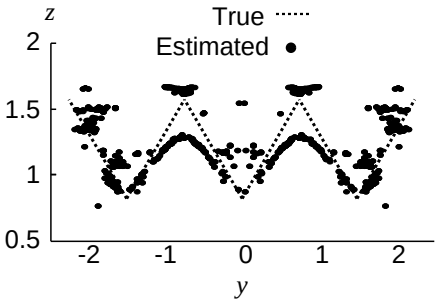

Fig. 2. Estimated target points with RPM and the Wiener filter for $-1.0 \leq x \leq 1.0$.

radius Z. It calculates (x, y, z) by investigating the distribution of intersection circles between the spheres determined with (X, Y, Z) and (X_i, Y_i, Z_i). Each intersection circle, projected to $z = 0$ plane, becomes a line defined as L_i. This method determines the target location (x, y) as

$$(x(\boldsymbol{q}), y(\boldsymbol{q})) = \arg\max_{x,y} \left| \sum_{i=1}^{N_{\mathrm{q}}} s(\boldsymbol{q}_i) \exp\left\{ -\frac{d\,(x, y, \boldsymbol{q}, \boldsymbol{q}_i)^2}{2\sigma_d^2} - \frac{D(\boldsymbol{q}, \boldsymbol{q}_i)^2}{2\sigma_D^2} \right\} \right|, \tag{1}$$

where $\boldsymbol{q} = (X, Y, Z)$, $\boldsymbol{q}_i = (X_i, Y_i, Z_i)$, and $d\,(x, y, \boldsymbol{q}, \boldsymbol{q}_i)$ denotes the minimum distance between the projected line L_i and $(x, y, 0)$. $D\,(\boldsymbol{q}, \boldsymbol{q}_i) = \sqrt{(X - X_i^2) + (Y - Y_i^2)}$, σ_d and σ_D are empirically determined. Under the assumption $z \geq 0$, the z coordinate of each target point is given by $z(\boldsymbol{q}) = \sqrt{Z^2 - \{x(\boldsymbol{q}) - X\}^2 - \{y(\boldsymbol{q}) - Y\}^2}$ This algorithm ignores the connecting procedures of a large number of range points, and then, it produces accurate target points, even if an extremely complicated range map is given. The detailed characteristic is described in [7].

The performance example of RPM is presented here, where the received electric field is calculated by the FDTD (Finite Difference Time Domain) method. The former study [7] employs the Wiener filter and the range points (X, Y, Z) are extracted from the local maxima of the output of this filter, which are beyond the determined threshold [7]. Fig. 2 shows the target points obtained with this method for the region $-1.0 \leq x \leq 1.0$, where the target boundary is assumed as in Fig. 1. Noiseless environment is assumed. The monostatic antenna is scanned for $-2.5 \leq x, y \leq 2.5$, where the number of locations on each axis are 51. $\sigma_d = 0.1\lambda$ and $\sigma_D = 0.6\lambda$ are set. This figure shows that the estimated target points suffers from a severe inaccuracy, and the produced target boundary is far from the actual one. This is because the obtained image with the RPM seriously depends on the accuracy for range points, which have non-negligible errors due to multiple interfered signals in the same range gate, or a scattered waveform deformation [9]. Then, an accurate and high resolution range extraction is imperative especially for the complex-shaped target imaging.

IV. Proposed Range Extraction Algorithm

To overcome the difficulty described above, this paper proposes a novel algorithm for range points extraction, by extending the Capon method. The Capon algorithm is one of the most powerful tools for enhancing range resolution based on frequency domain interferometry (FDI). It is confirmed, however, that the scattered waveform deformation distorts the range resolution and accuracy of the original Capon method. As a solution for this, the proposed method optimizes the reference signal used in the Capon. This method introduces a simplified waveform model, based on the fractional derivative of the transmitted waveform as,

$$S_{\mathrm{ref}}(\omega, \alpha) = (\mathrm{j}\omega)^{\alpha} S_{\mathrm{tr}}(\omega)^*, \tag{2}$$

where $S_{\mathrm{tr}}(\omega)$ is the transmitted signal in the angular frequency domain and * denotes a complex conjugate. α is a variable which satisfies $|\alpha| \leq 1$. It is confirmed that this simplified waveform model offers an accurate approximation to actual scattered one, where the range accuracy is estimated to be of the order of 0.01 λ in using the matched filter.

Based on this waveform model, the observed vector $\boldsymbol{V}_n(\alpha, \boldsymbol{L})$ is defined as,

$$\boldsymbol{V}_n(\alpha, \boldsymbol{L}) = \left[\frac{S(\omega_n, \boldsymbol{L})}{S_{\mathrm{ref}}(\omega_n, \alpha)}, \cdots, \frac{S(\omega_{n+M-1}, \boldsymbol{L})}{S_{\mathrm{ref}}(\omega_{n+M-1}, \alpha)} \right]^T, \tag{3}$$

where $S(\omega, \boldsymbol{L})$ denotes the received signal in angular frequency domain at $\boldsymbol{L} = (X, Y, 0)$, and M denotes the dimension of $\boldsymbol{V}_n(\alpha, \boldsymbol{L})$. Here, in order to suppress a range sidelobe caused by the coherent interference signal, the frequency averaging is applied. The averaged correlation matrix $\boldsymbol{R}(\alpha, \boldsymbol{L})$ is defined as,

$$\boldsymbol{R}(\alpha, \boldsymbol{L}) = \sum_{n=1}^{N-M+1} z_n \boldsymbol{V}_n(\alpha, \boldsymbol{L}) \boldsymbol{V}_n^H(\alpha, \boldsymbol{L}), \tag{4}$$

where ^{H} denotes the Hermitian transpose. N is the total number of the frequency points, and determined by the maximum frequency band of the transmitted signal. $M \leq N$ holds. z_n is defined as $z_n = 1/(N - M + 1)$, for simplicity. The output of the extended Capon $s_{\mathrm{cp}}(\alpha, Z', \boldsymbol{L})$ is defined as,

$$s_{\mathrm{cp}}(\alpha, Z', \boldsymbol{L}) = \frac{S_0^{-1}}{\boldsymbol{a}^H(Z') \boldsymbol{R}(\alpha, \boldsymbol{L})^{-1} \boldsymbol{a}(Z')}, \tag{5}$$

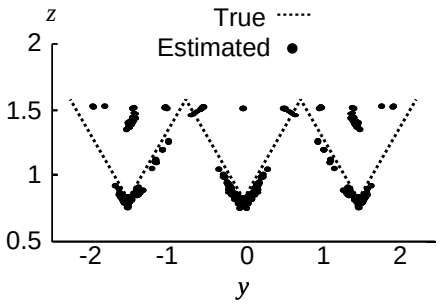

Fig. 3. Estimated target points with RPM and the extended Capon method for $-1.0 \leq x \leq 1.0$.

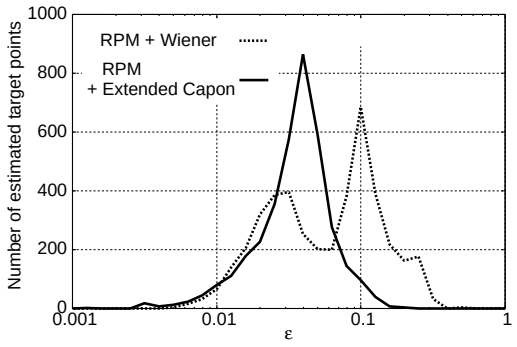

Fig. 4. Number of the target points for each ϵ.

where $\boldsymbol{a}(Z')$ denotes the steering vector of Z' as,

$$\boldsymbol{a}(Z') = \left[\mathrm{e}^{-\mathrm{j}\omega_1 2Z'\lambda/\mathrm{c}}, \mathrm{e}^{-\mathrm{j}\omega_2 2Z'\lambda/\mathrm{c}}, ..., \mathrm{e}^{-\mathrm{j}\omega_M 2Z'\lambda/\mathrm{c}}\right]^T. \quad (6)$$

S_0 is defined as

$$S_0 = \sqrt{\int \left\{\boldsymbol{a}^H(Z')\boldsymbol{R}(\alpha, \boldsymbol{L})^{-1}\boldsymbol{a}(Z')\right\}^{-2} \mathrm{d}Z'}. \quad (7)$$

The normalization with S_0 enables us to compare the amplitude of $s_{\mathrm{cp}}(\alpha, Z', \boldsymbol{L})$ respect to α. Then, the local maximum of $s_{\mathrm{cp}}(\alpha, Z', \boldsymbol{L})$ for α and Z' offers an optimized range resolution in the Capon method. Finally, it determines the range points (X, Y, Z), which satisfies the following conditions,

$$\left.\begin{array}{c} \partial s_{\mathrm{cp}}(\alpha, Z', \boldsymbol{L})/\partial\alpha = 0 \\ \partial s_{\mathrm{cp}}(\alpha, Z', \boldsymbol{L})/\partial Z' = 0 \\ s_{\mathrm{cp}}(\alpha, Z', \boldsymbol{L}) \geq \max_{Z'} \beta s_{\mathrm{cp}}(\alpha, Z', \boldsymbol{L}) \end{array}\right\}, \quad (8)$$

where β is empirically determined. This algorithm selects an accurate range point by enhancing the range resolution of the Capon method with the optimized reference signal. Each target point (x, y, z) is calculated from the group of range points in Eq. (1), that is the RPM.

V. Performance Evaluation

A. Numerical Simulation

Fig. 3 shows the estimated target points with RPM, when the extended Capon method is used for range extraction. The same data in Fig. 2 is used. Here, $N = 100$, $M = 20$ and $\beta = 0.3$ are set. It is confirmed that this method remarkably enhances the accuracy of the target points extraction especially for the convex edge region. This is because the output of the extended Capon offers a higher range resolution by suppressing the range sidelobe caused in using the Wiener filter, and enhances the accuracy by optimizing the reference waveform. Here, the deep-set concave boundary is not reconstructed, because the direct scattered signal from this region cannot be received at any antenna location. This is an inherent problem of RPM as far as a single scattered signal is used for imaging.

For the quantitatively analysis of each method, ϵ is introduced as

$$\epsilon(\boldsymbol{x}_{\mathrm{e}}^i) = \min_{\boldsymbol{x}_{\mathrm{true}}} \|\boldsymbol{x}_{\mathrm{true}} - \boldsymbol{x}_{\mathrm{e}}^i\|, \quad (i = 1, 2, ..., N_{\mathrm{T}}), \quad (9)$$

where $\boldsymbol{x}_{\mathrm{true}}$ and $\boldsymbol{x}_{\mathrm{e}}^i$ express the location of the true target point and that of the estimated point, respectively. N_{T} is the total number of $\boldsymbol{x}_{\mathrm{e}}^i$. Fig. 4 plots the number of the estimated points for each value of ϵ. This figure proves that the proposed method enhances the number of accurate target points around $\epsilon = 0.04\lambda$. The mean value of ϵ is $7.0 \times 10^{-2}\lambda$ for the Wiener filter and $3.5 \times 10^{-2}\lambda$ for the extended Capon. This result quantitatively proves that the proposed method accomplishes a super-resolution imaging beyond wavelength in terms of clear surface extraction.

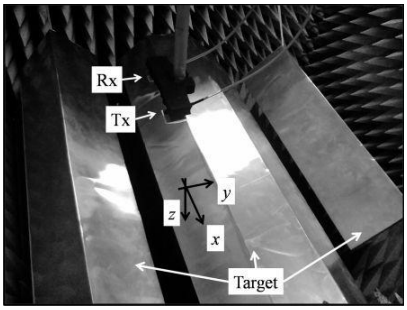

Fig. 5. Arrangement for multiple targets and UWB microstrip patch antennas.

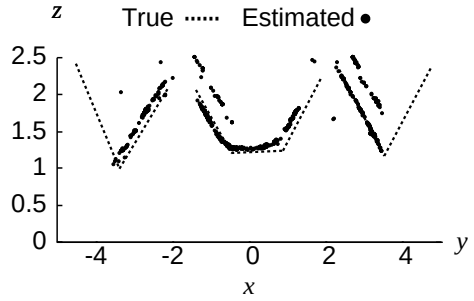

Fig. 6. Estimated target points obtained by RPM and the Wiener filter in the experiment for $-1.0 \leq y \leq 1.0$.

B. Experiment

This section investigates the experimental study of the proposed algorithm. We utilize a UWB pulse with a center frequency of 3.3 GHz and a 10dB-bandwidth of 3.0 GHz. The

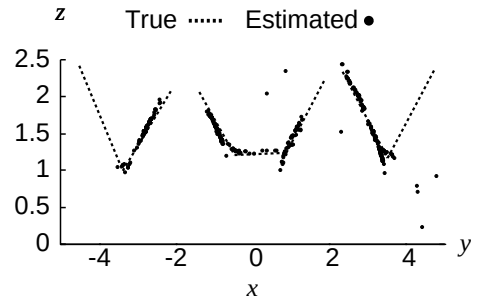

Fig. 7. Estimated target points obtained by RPM and the extended Capon method in the experiment for $-1.0 \leq y \leq 1.0$.

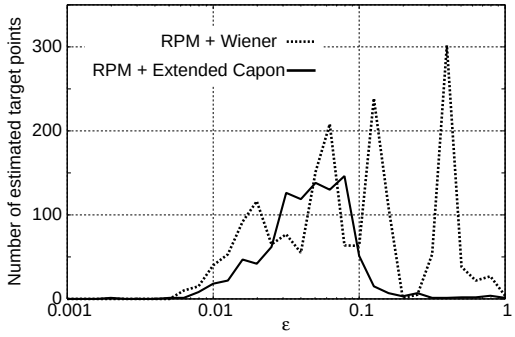

Fig. 8. Number of the target points for each ϵ in the experiment.

center wavelength, λ, of the pulse is 91 mm. The antenna has an elliptic polarization, of which the ratio of major to minor axes is about 17 dB, and the direction of the polarimetry axis of the antenna is along the y-axis. One trapezoid and two triangle prismatic targets are set, and are covered with 0.2 mm thick aluminum sheet. Fig. 5 illustrates the arrangement of antennas with respect to the the multiple targets. The transmitting and receiving antennas are scanned on the $z = 0$ plane, for $-3.3 \leq x \leq 3.3$ and $-1.1 \leq y \leq 1.1$, respectively, with both sampling intervals set to 0.11λ. The separation between the transmitting and receiving antennas is 1.4λ in the y-direction. The direct scattered signal from the targets can be obtained by eliminating the direct signal from the transmitting antenna.

Fig. 6 shows the extracted target points using the RPM for $-2.0 \leq y \leq 2.0$, when the Wiener filter is used for range extraction. The mean S/N is around 30 dB. Here, the bi-static extension of RPM is applied, where the target points are determined by the group of the intersection curves between ellipsoids whose foci are the locations of the transmitting and receiving antennas. This figure proves that the target points have non-negligible errors, especially around the trapezoid edge region. In addition, the unnecessary image appears above the actual boundary which is due to the range sidelobe of the Wiener filter. Fig. 7 shows the same view as in Fig. 6, when the extended Capon is applied for the range extraction. $N = 50$, $M = 10$ and $\beta = 0.3$ are set in this case. In this figure, it is confirmed that the target points accurately express a true target surface, including the edge region, and the false image due to the range sidelobe in the Wiener filter is significantly suppressed. This proves that the frequency domain interferometry using the Capon with the reference signal optimization enhances the accuracy and resolution for ranges, where the RPM offers an utmost performance and achieves super-resolution image even for complex-shaped 3-D objects. Fig. 8 shows the number of the target points with the sampled ϵ defined in Eq. (9) for each method. The method with the extended Capon increases the number of points with the accuracy around 0.05λ. The mean values of ϵ for each method are $1.49 \times 10^{-1}\lambda$ for the Wiener filter and $5.55 \times 10^{-2}\lambda$ for the extended Capon.

VI. Conclusion

This paper proposes a novel range extraction algorithm as the extended Capon method, known as the frequency domain interferometry. To enhance the image quality of the RPM, including the case for complicated shaped objects with concave or convex edges, this method optimizes the reference signal employing a simplified waveform model. It has a substantial advantage that the range resolution is remarkably enhanced, even if the different scattered waves are mixed together within the range scale less than wavelength. The results from numerical simulation and an experiment employing UWB modules verify that the combination with the extended Capon and RPM remarkably improves the accuracy for the target surface extraction, even for a complicated 3-D object including edges.

References

[1] D. L. Mensa, G. Heidbreder and G. Wade, "Aperture Synthesis by Object Rotation in Coherent Imaging," *IEEE Trans. Nuclear Science.*, vol. 27, no. 2, pp. 989–998, Apr, 1980.

[2] D. Liu, G. Kang, L. Li, Y. Chen, S. Vasudevan, W. Joines, Q. H. Liu, J. Krolik and L. Carin, "Electromagnetic time-reversal imaging of a target in a cluttered environment," *IEEE Trans. Antenna Propagat.*, vol. 53, no. 9, pp. 3058–3066, Sep, 2005.

[3] F. Soldovieri, A. Brancaccio, G. Prisco, G. Leone and R. Pieri, "A Kirchhoff-Based Shape Reconstruction Algorithm for the Multimonostatic Configuration: The Realistic Case of Buried Pipes," *IEEE Trans. Geosci. Remote Sens.*, vol. 46, no. 10, pp. 3031–3038, Oct, 2008

[4] T. Sakamoto, "A fast algorithm for 3-dimensional imaging with UWB pulse radar systems," *IEICE Trans. Commun.*, vol.E90-B, no.3, pp. 636–644, 2007.

[5] S. Kidera, T. Sakamoto and T. Sato, "High-Resolution and Real-time UWB Radar Imaging Algorithm with Direct Waveform Compensations," *IEEE Trans. Geosci. Remote Sens.*, vol. 46, no. 11, Oct., 2008.

[6] S. Kidera, T. Sakamoto and T. Sato, "High-Resolution 3-D Imaging Algorithm with an Envelope of Modified Spheres for UWB Through-the-Wall Radars," *IEEE Trans. Antenna & Propagat*, vol. 57, no. 11, pp. 3520–3529, Nov., 2009.

[7] S. Kidera, T. Sakamoto and T. Sato, "Accurate UWB Radar 3-D Imaging Algorithm for Complex Boundary without Range Points Connections," *IEEE Trans. Geosci. Remote Sens.*, vol. 48, no. 4, pp. 1993-2004, Apr., 2010.

[8] J. Capon, "High-resolution frequency-wavenumber spectrum analysis," *Proc. IEEE*, vol. 57, no. 8, pp. 1408–1418, Aug. 1969.

[9] S. Kidera, T. Sakamoto, T. Sato and S. Sugino, "An Accurate Imaging Algorithm with Scattered Waveform Estimation for UWB Pulse Radars", *IEICE Trans. Commun.*, vol. E89-B, no. 9, pp. 2588-2595, Sept., 2006